

MapperEEG: A Topological Approach to Brain State Clustering in EEG Recordings

Brittany Story^a, Zhibin Zhou^b, Ramesh Srinivasan^b, Piotr J. Franaszczuk^{a,c}

^a*U.S. Army DEVCOM Army Research Laboratory, 7101 Mulberry Point Rd, Aberdeen Proving Ground, 21005, MD, USA*

^b*University of California, Irvine 3151 Social Sciences Plaza, Irvine, 92617, CA, USA*

^c*Johns Hopkins University School of Medicine, 733 N Broadway, Baltimore, 21205, MD, USA*

Abstract

Electrical potential scalp recordings (Electroencephalograms-EEGs) are a common tool used to investigate brain activity. EEG is routinely used in clinical applications as well as in research studies thanks to its noninvasive nature, relatively inexpensive equipment, and high temporal resolution. But, EEG is prone to contamination from movement artifacts and signals from external sources. Thus, it requires advanced signal processing and mathematical analysis methods in tasks requiring brain state identification. Recently, tools from topological data analysis have been used successfully across many domains, including brain research, however these uses have been limited to fMRI datasets. We introduce the topological tool MapperEEG (M-EEG) and provide an example of its ability to separate different brain states during a simple finger tapping teaming task without any pre-labeling or prior knowledge. M-EEG uses the power spectral density applied to traditional EEG frequency bands combined with the Mapper algorithm from topological data analysis to capture the underlying structure of the data and represent that structure as a graph in two-dimensional space. This tool provides clear separation (clustering) of states during different conditions of the experiment (syncopated vs. synchronized) and we demonstrate that M-EEG outperforms other clustering methods when applied to EEG data.

1. Introduction

Characterizing normal and pathological brain states has long been a key component of neuroscience. One way to capture and analyze brain states is through an electroencephalogram (EEG). EEG data is easy to collect, inexpensive, non-invasive, and it provides high time resolution, which makes it a useful tool for researchers across a wide range of disciplines. It has some drawbacks such as low spatial resolution, high noise levels, and a high number of artifacts. Various analytical methods are used for interpretation of EEG data both for clinical and research applications. [1]. From the earliest EEG studies, clinicians and researchers noticed the presence of oscillatory features in EEG recordings. Over time, the oscillatory components of EEG within different frequency bands were correlated with certain brain functions and pathologies[2]. Other brain data collection methods, such as fMRI, were introduced later with higher spacial resolution and less noise, however, with lower time resolution and significantly higher costs. Recently, topological approaches have been used by computational neuroscientists to capture and cluster brain states. In [3], researchers studied the organization of brain states using an algorithm called Mapper, introduced by Singh et al. in [4]. Mapper, when applied to fMRI data, was able to organize different brain states categorically without any labeling. But, the types of tasks and states are limited to those that can be collected inside the laboratory setting with all additional restrictions imposed by fMRI. Thus, we look to see how we can use Mapper paired with tools from traditional EEG approaches to cluster EEG data to uncover the underlying structure of brain states.

In this work, we introduce MapperEEG (M-EEG), an approach for analyzing EEG data that uses the power spectral density function paired with the Mapper algorithm. We demonstrate how combining these approaches can be used to understand brain state structure by showing its efficacy at clustering brain states during a human teaming task. The paper is organized as follows. Section 3 outlines the M-EEG algorithm and why this approach is appropriate for EEG data. We also outline the dataset we used to test our algorithm. Next, Section 4 shows how M-EEG can be used to understand the

dataset’s structure and we verify M-EEG’s efficacy and utility. Finally, we discuss how M-EEG can be used with other datasets and consider possible extensions.

2. Background

2.1. EEG

Electroencephalography (EEG) has been a popular neuroimaging technique for understanding what goes on in the brain since it’s first human application in 1924. [5] Non-invasive, inexpensive, and EEG’s high-temporal resolution are a few of advantages it has to offer [6]. Modern systems can use anywhere from 4 to 256 electrodes, depending on the application and years of research has pinpointed the optimal electrode placement for a wide range of tasks, such as neural speech tracking, epilepsy, and concentration [7, 8, 9]. But there are some disadvantages, just as with any data collection approach. Lack of spatial resolution, individual brain and skull differences, depth restrictions and noise are just a few of the difficulties researchers face [10]. Over the years, researchers have worked around these obstacles and created tools that clean and parse EEG data. Source localization, band separation, filtering, down-sampling, and other signal processing techniques have allowed researchers to find meaningful patterns and information in the initially messy data [11]. One such task is the clustering of brain states.

Understanding how brain states differ across tasks has been explored across a variety of domains such as during transitions, resting, seizures, and mental tasks [12, 13, 14, 15]. Often, these approaches rely on other types of neuroimaging, such as fMRI. Thus, there is a need for a methodology that can classify different brain states across different task types with EEG data. Traditional methods such as event-related potentials and oscillatory dynamics have long been used to analyze and interpret EEG data [2]. More modern approaches such as Bayesian networks, support vector machines (SVMs), and random forests, characterize signals and associate them to behavior. For example, Bird et al. have used these methods to classify brain states as neutral, relaxed, or concentrating with an accuracy of roughly 87% [16]. EEG states have also been used as a method of communication for people with communication issues[17]. Additionally, EEG has been used to classify teammate trust with a decision tree classifier with an accuracy level of 72% [18]. Our goal is to develop an EEG clustering/mapping algorithm demonstrates solid accuracy while also capturing the relationship between states.

2.2. Mapper

The Mapper algorithm was first developed by Singh, Memoli, and Carlsson in 2007 as a way to visualize and understand the structure of high dimensional data[4]. Since it’s inception, it has been used in several different domains, such as fraud detection, gerrymandering, and neuroscience[19, 20, 21]. With respect to neuroscience, Mapper has been used to detect and identify transition states, pinpoint causal states, and predict states [22, 23, 24]. Other topological tools, such as persistent homology, have been used to look at simulated EEG data [25], cancer research [26], and brain injuries [27]. These applications all leverage topology’s ability to analyze data in a way that is structurally relevant. In this work, we will focus on using Mapper to examine the underlying structure of multiple EEG channels and how each state connects with the rest of the states.

3. Method: Applying Mapper to EEG Data

As a way to capture and cluster different brain states from EEG data, we look to the processes outlined in work such as those by Saggari, Geniesse, and others[3, 28, 22]. In each of these works, the researchers use Mapper as a way to characterize brain states based on fMRI data. To our knowledge, this analysis has been restricted to fMRI data. As such, we show that similar structure can be found in underlying EEG data. For this characterization, we look at EEG data from a finger tapping teaming task. Then we use EEG preprocessing paired with the Mapper algorithm to categorize brain states in a lower dimensional space. Below, we outline the dataset, preprocessing procedures, downsampling, and the Mapper algorithm.

3.1. Dataset

Neuroscientists have used synchronous/syncopated tapping tasks in a variety of ways. Mayville et al. used synchronized and syncopated tapping to study the cortical and subcortical networks in the brain [29] via fMRI data. Additionally, Mayville et al. have also studied how event-related changes in brain activity captured by Magnetoencephalography (MEG) are associated with synchronous and syncopated tapping [30]. But, both of these studies rely on MEG data and as such, we want to show that with M-EEG, EEG can also be used to differentiate between synchronization and syncopation.

For our analysis, we used data collected by Zhou, outlined in [31]. We have included a short summary of the data collection process and a description of the data for the reader, but for more information, see the paper cited above.

The experiment consisted of six pairs of tappers, a left and right tapper, isolated from each other. Each pair participated in two sessions, synchronized and syncopated. In the synchronized session, tappers tapped with the beat and with each other. The syncopated session consisted of tappers tapping between each beat, first with the metronome, then between whichever beat was provided. During each session, the tappers performed 12 trials with three instances of each of the four trial types semi-randomly shuffled. Each tapper initially paced off of a metronome set at 1.3 Hz (78 beats per minute) for the first 30 beats and then kept the beat after the metronome was removed.

For the first trial type, both tappers tapped independently, with no feedback from the other tapper. The second and third trial types, left lead and right lead, assigned one tapper (the leader) to synchronize/syncopate with the same metronome and the other tapper (the follower) to synchronize/syncopate with the leader via a visual cue. The fourth trial type consisted of bidirectional tapping; after the first 30 taps, each tapper was given visual feedback from the other tapper and the two tappers were told to synchronize/syncopate with each other’s tapping.

Each trial lasted ~ 3 minutes and consisted of 230 taps. The first 30 taps, which used the metronome, were removed from the dataset. Each session’s dataset includes 32 channels of EEG data sampled at 2000 Hz and 1 channel that recorded the button presses for each participant. Additionally, the dataset included the session type, trial type, and channel labels.

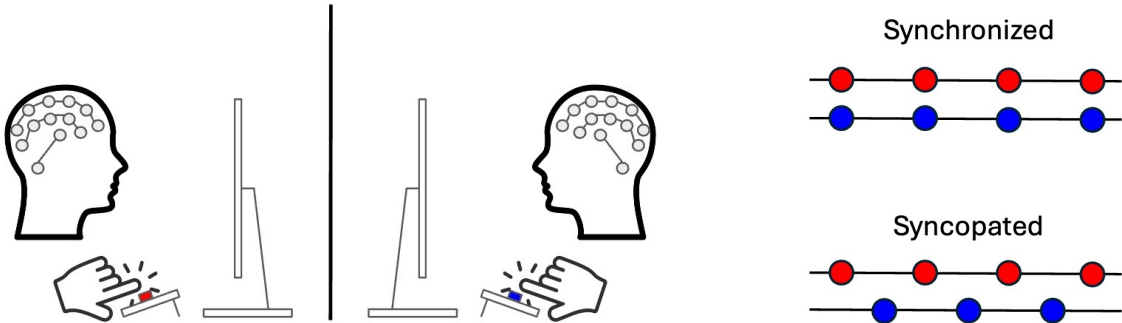


Figure 1: Left: A pair of tappers performing the tapping task. The tappers were isolated from each other, with feedback from the other tapper provided appropriately given the trial and session. Right: A comparison of synchronization and syncopation.

3.2. Preprocessing and Downsampling

Just as in [31], we preprocessed the data before it was fed into the Mapper algorithm. Double taps were removed if two or more taps happen within 350ms. Taps were extracted from the pairs of subjects based on the subject with the smallest number of taps. Preprocessing the EEG data consisted of filtering out the noise, detrending the data, re-referencing, and performing ICA to remove eye blinks. Finally, each session was chopped into trials and labeled appropriately.

Next, we downsampled each trial to reduce the size of the data, computation time, and to capture more relevant information. Each synchronized and syncopated dataset contained over 9 million and 3 million data points, respectively, with a sampling rate of 2000Hz. We applied a cutoff frequency filter of 50Hz and then downsampled each trial 2000Hz to 100Hz, in accordance with Nyquist’s theorem. This resulted in each trial consisting of 350 35-dimensional data points, 32 EEG channels, 1 response channel, trial type, and session type.

3.3. Power Spectral Density

In our approach, we rely on well investigated characteristics of EEG in the frequency domain. After the initial data cleaning and downsampling, we calculated the Power Spectral Density (PSD) for each channel using the `ss.welch` python function across different bands with a window size of 1000 samples and window overlap 50%. We calculated each channel’s PSD for each tapper and used a typical EEG bands of 1-4Hz (delta) 4-7Hz (theta), 8-12Hz (alpha) 13-30Hz (beta) 30Hz and beyond (gamma) as in [32, 33] to gain additional information about the brain activity, see Figure 2. As described in Paek et al. [34], brain activity that corresponds to finger movement lives in the delta band (1-3.5 Hz). This appears in the PSDs as a spike at approximately 1.3 Hz, the tapping frequency. As such, we applied M-EEG to each of the five bands to identify the band with the highest Q_{mod} score. After analyzing M-EEG outputs across the five different bands for each tapper, we use the power in gamma band as it resulted in highest average clustering accuracy across all tappers. We will elaborate on the clustering accuracy metric in Section 4.3.

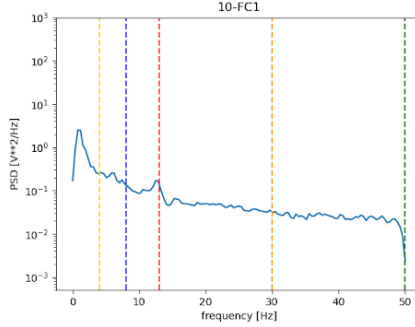


Figure 2: A graph of the PSD for channel 10-FC1 from a single tapper. Note, the largest spike corresponds to the frequency of the taps (1.3Hz).

3.4. Applying Mapper

After preprocessing, downsampling the data and converting it into the spectral domain, we fed it into the Mapper algorithm, first introduced in [4]. The Mapper package used, Kepler Mapper, is outlined in [35] and the code can be found in [36]. As outlined above in Section 3, we followed a similar pipeline as that shown in [3].

Before showing how M-EEG works, we give a simple example for how the Mapper algorithm works. Consider a set of data that falls in the shape of a circle, see Figure 3. First, we projected the points onto their y -coordinates on the y -axis. Next, we binned the points into three bins (red, yellow, blue) that overlapped by 33% (overlap denoted in orange and green). Then, we applied the bin labels to the points in their original space. Finally, we applied a clustering algorithm that groups together points based on their bin membership and their closeness to each other. Edges are drawn between any two nodes that contain points that are housed in both bins. This resulted in the graph on the far right of Figure 3, which captures the structure of the circle.

Thus, with that example in mind, we explain how we used Mapper to group brain states. First, we used t-SNE to project from the dataset’s base space (\mathbb{R}^{32}) into lower dimensional space (\mathbb{R}^3). Next, we chose the number of n -cubes and the amount of overlap desired to completely cover the lower dimensional space. We tested a range of cube numbers and overlap values outlined in Subsection 4.2 to ensure that the algorithm did not rely on cherry-picking parameters. Then, we used DBSCAN to cluster the data in \mathbb{R}^{32} based on the partitioning assigned in the projection space. Finally, we represented each cluster as a pie chart that shows the distribution of labels within the cluster. Similarly, we scaled each cluster based on the number of points it contained. For the M-EEG pipeline, see Figure 4.

4. Results

Below, we outline three different results. First, we demonstrate that the traditional Mapper approach does not yield useful results when applied to directly to the EEG timeseries. Conversely, we

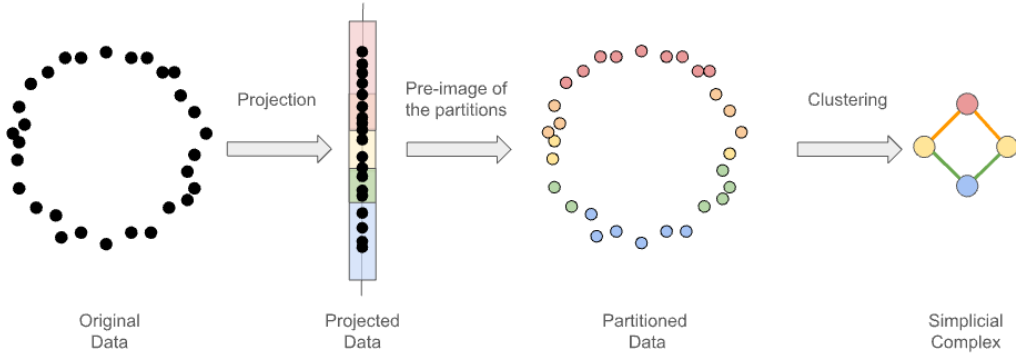


Figure 3: An example of the Mapper algorithm for a toy dataset. Note, the structure of the Mapper graph is the same as that of the dataset.

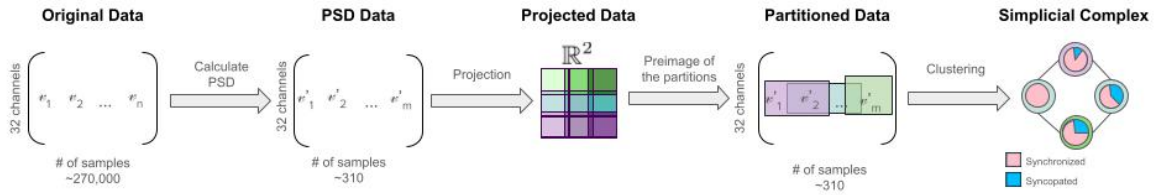


Figure 4: An example of the Mapper algorithm with projection function $T-SNE : \mathbb{R}^{32} \rightarrow \mathbb{R}^2$. We cover the 2-dimensional plane with boxes that overlap a certain amount. Then, we cluster points in \mathbb{R}^{32} based off the label assigned to the each of the points in the projection space and clustering-based distance. If points fall into two clusters, we denote this by connecting those clusters. Thus, we represent the structure of the data as the simplicial complex on the right side of the figure, which captures the relevant topological information.

show that Mapper works well in the frequency domain across the traditional EEG bands. Then, we show that M-EEG represents the data well by evaluating the Q_{mod} score across several different clustering algorithms. Finally, we compare M-EEG against other clustering algorithms using the F-1, Silhouette, and Davies-Bouldin metrics.

4.1. The Importance of the Spectral Domain

Since EEG’s foundation, researchers have used different techniques to transform data from the time domain to the spectral domain as a way to understand and find patterns in the data [37]. Unlike other data formats, such as fMRI, the temporal domain is dominated by noise and it makes it hard to identify patterns and other information. Thus, we show the efficacy of switching to the spectral domain on the tapping data outlined above.

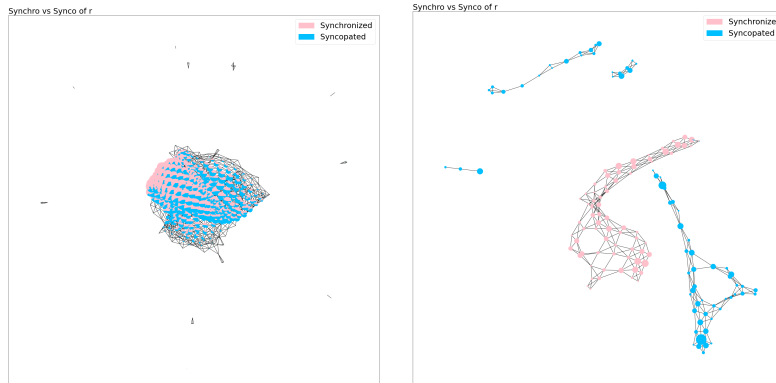


Figure 5: Both figures above were generated using the same data. Left: Temporal data. Right: The temporal data was converted to the spectral domain, as described in Section 3. As seen in the figure on the right, the Mapper algorithm naturally partitions the spectral data into different clusters which align with the synchronization and syncopation labels.

As seen in the left image of Figure 5, applying Mapper to the raw downsampled data yields a messy point cloud with no apparent organization. But, applying Mapper to the data after transforming it into the spectral domain yields two distinct clusters. After we impose the synchronization and syncopation labels, it is clear that Mapper is able to cluster the data appropriately, whereas it was not able to before. Now that we have established the importance of moving into the spectral domain, we show that M-EEG captures this underlying structure across a large range of parameters.

4.2. Analyzing the Community Structure of the Graph

Next, we seek to identify what are “good” graphs, a label that is ambiguous, so we turn to modularity, specifically the Q_{mod} function, to define what good means in this context. Garcia et al. summarize how modularity has provided valuable insight into task performance, memory performance, and working memory [38]. The Q_{mod} function captures the modularity of the graph by assigning a value between $(-\infty, 1)$. A value of 1 represents a perfectly modular graph where all like vertices are connected to other like vertices there are no connections between any dissimilar vertices. A graph with $Q_{mod} \approx 0$ captures the community structure of a graph where vertices are connected to like and different vertices randomly. A graph with $Q_{mod} < 0$ has less than expected edges of like vertices connected to like vertices and/or vertices connected to vertices with different labels. We use the Q_{mod} function mentioned in these works ([39, 40]) similar to how it was applied in [3]. Let $G = \{V, E\}$ be the Mapper graph generated by the M-EEG method outlined above. Thus,

$$Q_{mod} = \sum_{ij \in E} \left[A_{ij} - \frac{k_i k_j}{2m} \right] \delta(C_i, C_j),$$

where A_{ij} is the adjacency matrix entry for row i column j and m is the number of edges in the graph. For our purposes, k_i denotes the strength of node v_i , which we assign to be degree of v_i . The community of the node, C_i , is the majority of labels within a node. Note, labels can be pulled from the trial type, independent, leader, follower, or bidirectional, or the session type, synchronized or syncopated. If the labels are evenly split, we randomly select one from the majority. Finally, the function $\delta(C_i, C_j)$ is 1 when the labels match and 0 otherwise. [40]

We also use the Q_{mod} function as a way to test the effect of Mapper parameters and the choice of frequency band on the output graphs. M-EEG was applied to each participant’s sessions across a range of parameters. We performed a grid search across different numbers of cubes, [10, 15, 20, 25, 30, 35, 40], overlap proportions, [0.05, 0.1, 0.15, 0.2, 0.25, 0.3, 0.35, 0.4, 0.45, 0.5], and the five frequency bands, [1-4Hz (delta), 4-7Hz (theta), 8-12Hz (alpha), 13-30Hz (beta), 30+Hz (gamma)]. For a summary of the results of the hyperparameter search, see Figure 6. This allowed us to show that the community structure holds across different Mapper parameters, and identify the parameters that resulted in the highest Q_{mod} score for each participant. We calculated the Q_{mod} score with respect to the synchronized versus syncopated sessions.

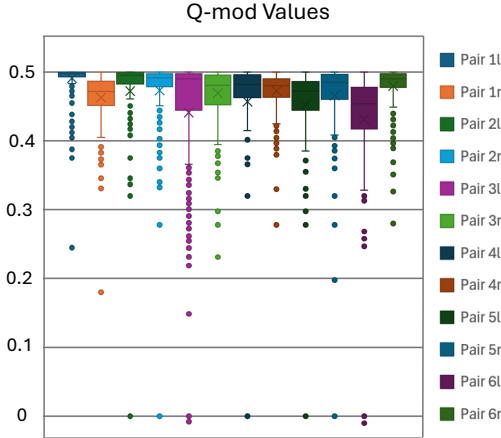


Figure 6: A box and whisker plot of all Q_{mod} scores for a grid search over different numbers of cubes, overlap amounts, and EEG bands for each tapper.

All average Q_{mod} scores are above 0.4, significantly higher than the 0 expected from a random dataset. This demonstrates that M-EEG produces graphs with high community structure. Additionally, since good community structure appears across a wide range of parameters, this supports that the M-EEG algorithm captures underlying structural information. We also look at Mapper’s application across the five frequency bands. All five bands produce an average across all tapper Q_{mod} score greater than 0.48, showing that Mapper is able to capture relevant information across all bands, see Table 1. Additionally, we see state separation across all five bands, see Figure 7.

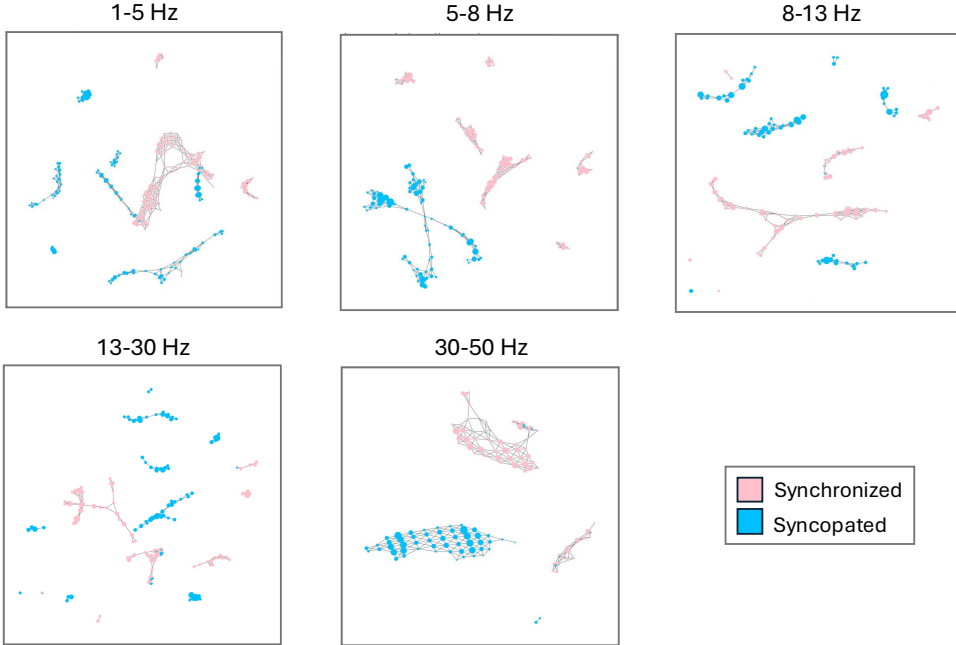


Figure 7: An example of the Mapper graphs of a single tapper across the five different frequency bands. Note, each separates the data into clusters that respect the synchronized/syncopated labeling.

| Band | 1-5 Hz (δ) | 5-8 Hz (θ) | 8-13 Hz (α) | 13-30 Hz (β) | 30-50 Hz (γ) |
|----------------|---------------------|---------------------|----------------------|----------------------|-----------------------|
| Cubes | 40 | 30 | 40 | 40 | 40 |
| Overlap | 0.5 | 0.45 | 0.4 | 0.45 | 0.45 |
| Avg. Q_{mod} | 0.4832 | 0.4916 | 0.4892 | 0.4923 | 0.4955 |

Table 1: A table outlining different parameters that yielded the highest average Q_{mod} across all 12 tappers.

4.3. Comparing Mapper Against Other Clustering Algorithms

Finally, we analyze how Mapper performs as a clustering algorithm. The goal of this task was to quantify how well Mapper clustered states correctly as synchronized or syncopated. To convert Mapper into a clustering algorithm, we identified each connected component as a cluster and assigned each of them label. We assigned the cluster that contained the first point with label 1 (synchronized) and the next largest cluster with label 2 (syncopated) to ensure labeling consistency. Some points did not appear in the Mapper graph, so we added an additional cluster for those points, much as how some points are assigned to the noise cluster in the DBSCAN algorithm. Note, each element of our dataset is assigned to a single component as an edge is drawn between two nodes if the nodes contain at least one of the same data point. Thus, the only way an element can be in multiple graph nodes is if they’re a part of the same component.

We tested Mapper against three common clustering algorithms across five different error measures, f1 micro (accuracy), f1 macro, f1 weighted, silhouette score, and Davies-Bouldin. For each algorithm, we did a hyperparameter search across a range of values, and identified the hyperparameters that yielded the highest average accuracy across all participants. For DBSCAN, we allowed the minimum

number of samples (ms) to range between [3, 20] and the maximum distance between samples of the same cluster (eps) between [5, 20]. For k -Means the user must choose the number of clusters, so we varied our clusters between [2, 10]. Similarly, for the Gaussian Mixture method (GMM), we looked across [2, 10] clusters and across four coverage types, [full, tied, diag, sphere]. The results for the parameters that yield the best average accuracy error across all participants are included in Table 2, where the second row states the hyperparameters that correspond to that accuracy measurement.

| Error/Algorithm | DBSCAN | k-Means | Gaussian Mix | M-EEG |
|-----------------|-------------------|------------|-------------------------|-------------------------|
| Parameters | $ms = 5, ep = 20$ | $clus = 2$ | $comps = 2, var = full$ | $cbs = 15, ovlp = 50\%$ |
| Band | beta | gamma | theta | alpha |
| Accuracy | 0.4383 | 0.5397 | 0.5441 | 0.7901 |
| F-1 Macro | 0.2161 | 0.4399 | 0.4195 | 0.5790 |
| F-1 Weighted | 0.3227 | 0.4390 | 0.4190 | 0.7893 |
| Silhouette | 0.6507 | 0.6818 | 0.8033 | 0.2015 |
| Davies-Bouldin | 1.2405 | 0.8383 | 0.7185 | 1.7552 |

Table 2: The average errors for each of the four clustering algorithms. Best scores are bolded for ease of comparison.

M-EEG outperformed the other algorithms across the first three error functions. These errors are calculated by comparing the true label list to the predicted label list and capture M-EEG’s accuracy. The last two scores focus on different ideas. The silhouette score calculates the distance between a sample and the nearest cluster that the sample is not a part of. The Davies-Bouldin score evaluates the ratio of within-cluster distances to between-cluster distances which means clusters that are farther apart and less dispersed will result in a better score. Both of these metrics have to do with evaluating how the algorithm clusters data in the data’s domain (\mathbb{R}^{32}). Since M-EEG projects the data and calculates the labels based off of those projections, M-EEG is capturing structure that is not strictly dependent on how close the points are in \mathbb{R}^{32} . So even though M-EEG has a worse Silhouette and Davies-Bouldin score than GMM, M-EEG’s clustering accuracy is 25% higher than GMM’s. This shows that the M-EEG algorithm is capturing structure that is not easily identified in the higher dimensional space.

5. Discussion

This work focused on introducing the M-EEG method as a topological approach to analyzing EEG data, specifically it’s ability to cluster brain states in a structurally relevant way. We focused this introduction on identifying the differences between individual brain states characterized by EEG recordings between two different experimental conditions; synchronized and syncopated finger tapping. However, applying the Mapper algorithm directly to the EEG time series did not separate brain states during the different conditions of the experiment. Only after performing spectral analysis of the EEG data and using power within different EEG spectral bands could we successfully cluster data into groups associated with the syncopated and synchronized conditions. Additionally, Mayville et al. [30] show that syncopation results in lower MEG power within the beta band. But, we found that M-EEG was able to cluster the syncopated and synchronized data across all bands, with the following corresponding accuracy values (in decreasing order); alpha: 0.7901, gamma: 0.7797, beta: 0.7515, theta: 0.7429, and delta: 0.6419. This demonstrates that there is not a huge significance between the alpha, gamma, beta, and theta bands. But, there is a significant difference between those four bands and the delta band. This, in part, could be the affect of the tapping on the delta band, as described in Subsection 4.1 and in [34]. Finally, we also showed in Table 1, that the Q_{mod} scores across all bands are within ~ 0.1 of each other, showing that all bands can produce graphs with high community structure.

The results in [3] show how Mapper is able to capture transition paths between brain states. Our future work looks at investigating whether the same kinds of transitions found within fMRI data can be captured with EEG. Specifically, we want to explore how nodes are connected with respect to time to see how states transition across time. For this, we plan to examine a new dataset that records both tasks and the times between tasks. Additionally, we plan to separately analyze data from individual EEG channels and look at how source localization might provide more information on brain state.

The ability to capture and understand brain state connectivity will provide researchers with insight into how the brain distributes tasks across different parts of the brain. This will help identify individuals who have high compartmentalization levels and allow us to compare the underlying brain structure across individuals. For example, some participant’s M-EEG graphs had higher average Q_{mod} scores across different M-EEG parameters, such as Tappers 1, 5, and 9 whereas others, such as Tapper 10 demonstrate significantly lower average Q_{mod} scores (see Figure 6). Finding that some of these individuals have more community structure than others might allow us to better understand why some people do better at some tasks than others. Moving forward, we plan to continue to use M-EEG to explore brain state connectivity and we hope to use that knowledge to understand and/or predict an individual’s brain state during a task. With the work outlined above, we have shown the potential M-EEG has to accomplish these goals.

6. Conclusion

Capturing the underlying structure of brain states is an ongoing endeavor. Tools that allow us to visualize connectivity and structure without relying on known labels provide researchers with an insight into brain state relationships. In the work above, we demonstrate that M-EEG produces brain state connectivity graphs with significant community structure by producing a high Q_{mod} value across a range of Mapper values. Additionally, M-EEG demonstrated its effectiveness as a clustering algorithm as it outperformed DBSCAN, k -Means, and the Gaussian Mixture Method by over 20% with respect to accuracy. These two pieces show that M-EEG has the potential to be a useful structural assessment and visualization tool for analyzing EEG data.

References

- [1] Peter W. Kaplan, Selim R. Benbadis, Aatif M. Husain, and William O. Tatum. *Handbook of EEG Interpretation*. Springer Publishing Company, 2007.
- [2] Gyorgy Buzsaki. *Rhythms of the Brain*. Oxford University Press, 10 2006.
- [3] Manish Saggar, Olaf Sporns, Javier Gonzalez-Castillo, and et al. Towards a new approach to reveal dynamical organization of the brain using topological data analysis. *Nature Communications*, 9:1399, 2018.
- [4] Gurjeet Singh, Facundo Memoli, and Gunnar Carlsson. Topological methods for the analysis of high dimensional data sets and 3d object recognition. In M. Botsch, R. Pajarola, B. Chen, and M. Zwicker, editors, *Eurographics Symposium on Point-Based Graphics*. The Eurographics Association, 2007.
- [5] Erik K St. Louis, Lauren C Frey, Jeffrey W Britton, Jennifer L Hopp, Pearce Korb, Mohamad Z Koubeissi, William E Lievens, and Elia M Pestana-Knight. *Electroencephalography (EEG): An Introductory Text and Atlas of Normal and Abnormal Findings in Adults, Children, and Infants*. American Epilepsy Society, 2016.
- [6] Bin He, Abbas Sohrabpour, Emery Brown, and Zhongming Liu. Electrophysiological source imaging: A noninvasive window to brain dynamics. *Annual review of biomedical engineering*, 2018.
- [7] Jair Montoya-Martínez, Jonas Vanthornhout, Alexander Bertrand, and Tom Francart. Effect of number and placement of eeg electrodes on measurement of neural tracking of speech. *PloS one*, 16, 2021.
- [8] Christina Maher, Yikai Yang, Nhan Duy Truong, Chenyu Wang, Armin Nikpour, and Omid Kavehei. Seizure detection with reduced electroencephalogram channels: research trends and outlook. *Royal Society open science*, 10, 2023.
- [9] Hossein Siamaknejad, Wei Shiung Liew, and Chu Kiong Loo. Fractal dimension methods to determine optimum eeg electrode placement for concentration estimation. *Neural Computing and Applications*, 31, 2019.

- [10] Leigh R Hochberg and John P Donoghue. Sensors for brain-computer interfaces. *IEEE Engineering in Medicine and Biology Magazine*, 25(5):32–38, 2006.
- [11] Li Hu and Zhiguo Zhang, editors. *EEG Signal Processing and Feature Extraction*. Springer, Singapore, 2019.
- [12] Morten L. Kringelbach and Gustavo Deco. Brain states and transitions: Insights from computational neuroscience. *Cell Reports*, 32(10):108128, 2020.
- [13] Megan H Lee, Carl D Hacker, Abraham Z Snyder, Maurizio Corbetta, Dongyang Zhang, Eric C Leuthardt, and Joshua S Shimony. Clustering of resting state networks. *PLoS One*, 7(7):e40370, Jul 2012.
- [14] Maria Centeno and David W Carmichael. Network connectivity in epilepsy: resting state fmri and eeg-fmri contributions. *Front. Neurol.*, 5:93, July 2014.
- [15] Emily S. Finn, Dustin Scheinost, Daniel M. Finn, Xilin Shen, Xenophon Papademetris, and R. Todd Constable. Can brain state be manipulated to emphasize individual differences in functional connectivity? *NeuroImage*, 160:140–151, 2017. Functional Architecture of the Brain.
- [16] Jordan J. Bird, Luis J. Manso, Eduardo P. Ribeiro, Anikó Ekárt, and Diego R. Faria. A study on mental state classification using eeg-based brain-machine interface. In *2018 International Conference on Intelligent Systems (IS)*, pages 795–800, 2018.
- [17] Ioulietta Lazarou, Spiros Nikolopoulos, Panagiotis C. Petrantonakis, Ioannis Kompatsiaris, and Magda Tsolaki. Eeg-based brain-computer interfaces for communication and rehabilitation of people with motor impairment: A novel approach of the 21st century. *Frontiers in Human Neuroscience*, 12, 2018.
- [18] Kazi Farzana Firoz, Younho Seong, and Seeung Oh. A neurological approach to classify trust through eeg signals using machine learning techniques. In *2022 IEEE 3rd International Conference on Human-Machine Systems (ICHMS)*, pages 1–6, 2022.
- [19] Satanik Mitra and Kameshwar Rao JV. Experiments on fraud detection use case with qml and tda mapper. In *2021 IEEE International Conference on Quantum Computing and Engineering (QCE)*, pages 471–472, 2021.
- [20] J. Thatcher, D. Retchless, C. Thatcher, and K. Jones. Putting mapper on a map: cartographic visualizations of topological data analysis. *Abstracts of the ICA*, 3:288, 2021.
- [21] Daniel Hasegan, Caleb Geniesse, Samir Chowdhury, and Manish Saggarr. Deconstructing the mapper algorithm to extract richer topological and temporal features from functional neuroimaging data. *Network Neuroscience*, pages 1–28, 10 2024.
- [22] Carter Geniesse, Olaf Sporns, Gergely Petri, and Manish Saggarr. Generating dynamical neuroimaging spatiotemporal representations (dyneur) using topological data analysis. *Network Neuroscience*, 3(3):763–778, 2019.
- [23] Emma Tassi, Harrison Fisher, Andrew Bolender, Jun-Hwan Lee, Lizbeth J. Ayoub, Anna Maria Bianchi, Braden Kuo, Vitaly Napadow, Eleonora Maggioni, and Roberta Sclocco. Topological data analysis of resting-state fmri suggests altered brain network topology in functional dyspepsia: A mapper-based parcellation approach. In Chao Chen, Yash Singh, and Xiaoling Hu, editors, *Topology- and Graph-Informed Imaging Informatics*, pages 88–99, Cham, 2025. Springer Nature Switzerland.
- [24] Stefano Vannoni, Emma Tassi, Inês Won Sampaio, and Eleonora Maggioni. Exploitation of mapper algorithm in neuroimaging applications: A novel framework for outcomes prediction. In Chao Chen, Yash Singh, and Xiaoling Hu, editors, *Topology- and Graph-Informed Imaging Informatics*, pages 76–87, Cham, 2025. Springer Nature Switzerland.
- [25] Farzana Nasrin, Christopher Oballe, David Boothe, and Vasileios Maroulas. Bayesian topological learning for brain state classification. pages 1247–1252, 12 2019.

- [26] Ciara F Loughrey, Pdraig Fitzpatrick, Nick Orr, and Anna Jurek-Loughrey. The topology of data: opportunities for cancer research. *Bioinformatics*, 37(19):3091–3098, 07 2021.
- [27] Jessica L Nielson, Jesse Paquette, Aiwen W Liu, Cristian F Guandique, C Amy Tovar, Tomoo Inoue, Karen-Amanda Irvine, John C Gensel, Jennifer Kloke, Tanya C Petrossian, Pek Y Lum, Gunnar E Carlsson, Geoffrey T Manley, Wise Young, Michael S Beattie, Jacqueline C Bresnahan, and Adam R Ferguson. Topological data analysis for discovery in preclinical spinal cord injury and traumatic brain injury. *Nat. Commun.*, 6(1):8581, October 2015.
- [28] Manish Saggar, James M. Shine, Raphaël Liégeois, and et al. Precision dynamical mapping using topological data analysis reveals a hub-like transition state at rest. *Nature Communications*, 13:4791, 2022.
- [29] Justine M Mayville, Kelly J Jantzen, Armin Fuchs, Fred L Steinberg, and J A Scott Kelso. Cortical and subcortical networks underlying syncopated and synchronized coordination revealed using fmri. *Hum. Brain Mapp.*, 17(4):214–229, December 2002.
- [30] J M Mayville, A Fuchs, M Ding, D Cheyne, L Deecke, and J A Kelso. Event-related changes in neuromagnetic activity associated with syncopation and synchronization timing tasks. *Hum. Brain Mapp.*, 14(2):65–80, October 2001.
- [31] Italo Ivo Lima Dias Pinto, Zhibin Zhou, Javier O. Garcia, and Ramesh Srinivasan. Symbolic dynamics of joint brain states during dyadic coordination, 2024.
- [32] Chetan S Nayak and Arayamparambil C Anilkumar. Eeg normal waveforms. In *StatPearls*. StatPearls Publishing, Treasure Island (FL), jan 2025.
- [33] Laurent Vézard, Pierrick Legrand, Marie Chavent, Frédérique Faïta-Aïnseba, and Leonardo Trujillo. Eeg classification for the detection of mental states. *Applied Soft Computing*, 32:113–131, 2015.
- [34] Andrew Paek, Harshavardhan Agashe, and Jose Contreras-Vidal. Decoding repetitive finger movements with brain activity acquired via non-invasive electroencephalography. *Frontiers in Neuroengineering*, 7, 2014.
- [35] Hendrik Jacob van Veen, Nathaniel Saul, David Eargle, and Sam W. Mangham. Kepler mapper: A flexible python implementation of the mapper algorithm. *Journal of Open Source Software*, 4(42):1315, 2019.
- [36] Hendrik Jacob van Veen, Nathaniel Saul, David Eargle, and Sam W. Mangham. Kepler Mapper: A flexible Python implementation of the Mapper algorithm, Oct 2020.
- [37] Marcus C Ng, Jin Jing, and M Brandon Westover. A primer on EEG spectrograms. *Journal of Clinical Neurophysiology*, 39(3):177–183, mar 2022.
- [38] Javier O. Garcia, Arian Ashourvan, Sarah Muldoon, Jean M. Vettel, and Danielle S. Bassett. Applications of community detection techniques to brain graphs: Algorithmic considerations and implications for neural function. *Proceedings of the IEEE*, 106(5):846–867, 2018.
- [39] M. E. J. Newman and M. Girvan. Finding and evaluating community structure in networks. *Phys. Rev. E*, 69:026113, Feb 2004.
- [40] Santo Fortunato. Community detection in graphs. *Physics Reports*, 486(3):75–174, 2010.